Reversibility of Ferri-/Ferrocyanide Redox during Operando Soft X-ray Spectroscopy

Citation: Risch, Marcel, Kelsey A. Stoerzinger, Tom Z. Regier, Derek Peak, Sayed Youssef Sayed, and Yang Shao-Horn. "Reversibility of Ferri-/Ferrocyanide Redox During Operando Soft X-Ray Spectroscopy." The Journal of Physical Chemistry C 119, no. 33 (August 20, 2015): 18903–18910.

As Published: http://dx.doi.org/10.1021/acs.jpcc.5b04609

Publisher: American Chemical Society (ACS)

Persistent URL: http://hdl.handle.net/1721.1/109590

Version: Author's final manuscript: final author's manuscript post peer review, without publisher's formatting or copy editing

Reversibility of Ferri-Ferrocyanide Redox During Operando Soft X-Ray Spectroscopy

Marcel Risch,[†*] *Kelsey A. Stoerzinger,*[§] *Tom Z. Regier,*[‡] *Derek Peak,*[º] *Sayed Youssef Sayed,*[†⊥] *Yang Shao-Horn*[†§||*]

[†]Research Laboratory of Electronics, Massachusetts Institute of Technology, Cambridge, MA, USA 02139

[§]Department of Materials Science and Engineering, Massachusetts Institute of Technology, Cambridge, MA, USA 02139

[||]Department of Mechanical Engineering, Massachusetts Institute of Technology, Cambridge, MA, USA 02139

[‡]Canadian Light Source, Inc., Saskatoon, SK, Canada S7N 2V3

ºDepartment of Soil Sciences, University of Saskatchewan, Saskatoon, SK, Canada S7N 5A8

KEYWORDS. Electrochemistry; In-situ; redox shuttle; iron cyanide; X-ray absorption; radiolysis; radiation damage.

ABSTRACT

The ferri-ferrocyanide redox couple is ubiquitous in many fields of physical chemistry. We studied its photochemical response to intense synchrotron radiation by in-situ X-Ray absorption spectroscopy. For photon flux densities equal to and above 2×10^{11} $s^{-1}mm^{-2}$, precipitation of ferric (hydr)oxide from both ferricyanide and ferrocyanide solutions was clearly detectable despite flowing fast enough to replace the solution in the flow cell every 0.4 s (flow rate 1.5 ml/min). During cyclic voltammetry, precipitation of ferric (hydr)oxide was promoted at reducing voltages and observed below 10^{11} $s^{-1}mm^{-2}$. This was accompanied by inhibition of the ferri-ferrocyanide redox, which we probed by time-resolved operando X-ray absorption spectroscopy. Our study highlights the importance of considering both electrochemical and spectroscopic conditions when designing in-situ experiments.

Introduction

Ferri-ferrocyanide is a common facile redox couple[1-3] that is frequently used to access surface charge transfer kinetics.[4-7] It is also an important component of diverse applications, including in charge storage within flow batteries,[8] as the electroactive species in thermogalvanic cells,[9-11] a preventor of electrolyte decomposition in batteries,[12] and as the redox shuttle in dye-sensitized solar cells[13] and photoanodes.[14] Previously, the redox of ferricyanide and ferrocyanide has been studied by hard and soft in-situ X-ray absorption spectroscopy (XAS) to elucidate photo-excitation,[15-16] chemical reduction,[17] solvation,[18-19] and charge transfer.[20] The attenuation length of hard X-rays at the Fe K-edge (7112 eV) is ~100× larger than that of soft X-rays at the Fe L_3-edge (706.8 eV),[21] which enlarges the irradiated mass by a factor of ~ 100 for hard X-rays, while the energies differ by a factor of ~ 10. The dose (energy deposited per mass) within one absorption

length is then about 10× larger at the Fe L_3-edge as compared to the Fe K-edge for a fixed number of incident photons. (Exact calculation gives 6.6× larger dose.[22]) Therefore, less radiation damage can be expected at the Fe K-edge as compared to the Fe L_3-edge. Yet there is little discussion of photochemical effects on the stability of ferricyanide and ferrocyanide during operando XAS with soft X-ray radiation. Moreover, Ferricyanide and ferrocyanide complexes can become unstable due to CN cleavage under UV illumination,[23] and electron irradiation,[24-26] especially at high pH.[27] These interactions lead to drastically reduced kinetics after few hours of operation,[28] which is commonly explained by precipitation of coordination polymers related to Prussian Blue[28-31] (ferric hexacyanoferrate) with general formula $A_hFe_k[FeCN]_l \cdot mH_2O$,[32] where A is a group I metal and h, k, l, m are stoichiometric indices.

Here, we studied the implications of ionizing radiation on ferricyanide and ferrocyanide complexes during open-circuit and cyclic voltammetry using soft XAS. Our experimental setup allows studying reactions within the bulk electrolyte and any side reactions occurring at the surface of the working electrode. This is in contrast to previous studies of iron sulfate redox in the bulk electrolyte,[33] where surface reactions at the working electrode are not probed by XAS (Figure S1). We find the threshold photon flux that can trigger the radiolysis of ferricyanide to form ferric (hydr)oxide at the electrode surface under open-circuit. Conducting cyclic voltammetry below the threshold photon flux resulted in the precipitation of ferric (hydr)oxide and electrode passivation in the irradiated area. Our work highlights the importance of considering both photochemical and electrochemical damage when designing electrochemical operando XAS experiments.

Experimental

X-ray absorption spectroscopy

X-ray absorption measurements at the iron *L*-edges were performed at the spherical grating monochromator (SGM) beamline 11ID-1 at the Canadian Light Source.[34] The window of the sample cells was mounted at an angle of roughly 45° with respect to both the incident beam and the detectors.[35] The irradiated area on the cell window was about 0.05 mm^2 as determined by image analysis in Adobe Photoshop (Figure S2). All measurements were made at room temperature in the fluorescence mode using Amptek silicon drift detectors (SDD) with 1024 emission channels (energy resolution ~120 eV). Four SDD were employed simultaneously; two detectors had vanadium (200 nm) and two detectors had titanium (200 nm) filter foils mounted to suppress the oxygen fluorescence. The partial fluorescence yield (PFY) was extracted from all SDDs by summation of the iron *L* emission lines between 664 and 872 eV. The PFY spectra were normalized for the background due to oxygen absorption by fitting a straight line in an appropriate region below the L_3-edge (typically between 695 and 703 eV) and subtracting it over the whole range of the data (685-755 eV) as shown in Figure S3A. The noise level of some spectra required adjustment of the boundaries so that the post-edge slope matched the pre-edge slope reasonably well. Finally, the average intensity between 732 and 735.5 eV (after L_2 edge) was normalized to unity (Figure S3B). The energy axis was calibrated with respect to the pre-edge in the spectrum of molecular oxygen at 530.8 eV,[36] which was acquired using a sample cell filled with ambient air. The incident intensity was obtained by measuring the current on a gold grid placed before the sample chamber. The absolute incident flux of 1×10^{10} photons/s was measured using a photodiode (IRD AXUV100) for a beamline exit slit size of 10 μm.[37] We assumed a linear dependence of the current on the gold grid and the photon flux within the used

range of 50% to 150% flux. Flux densities were obtained by division of the irradiated area on the cell window (0.05 mm^2).

In the ionic limit relevant to *L*-edge spectroscopy of iron, the spectral features are dominated by multiplet interactions between the ground, excited and relaxed electronic states,[38] which can provide a fingerprint for ferri- and ferrocyanide that can be assigned uniquely to an electronic configuration, e.g., $t_{2g}^5 e_g^0$. The iron *L*-edge spectra of ferricyanide, $[Fe^{III}(CN)_6]^{3-}$, and ferrocyanide, $[Fe^{II}(CN)_6]^{4-}$, have been analyzed in detail by theoretical methods[19, 39] and complementary experiments using high-resolution resonant inelastic X-ray scattering (RIXS).[18, 40]

Sample cell

The bodies of the sample cells were fabricated on an Object Connex500 printer by 3D printing with DurusWhite material (Figure 1). The design of the electrochemical flow cell was adapted from a previously used flow cell.[41] Silicon nitride membrane windows (1 mm x 1 mm x 100 nm) in Si frames (5 mm x 5 mm x 525 μm) were purchased from Silson or SPI Supplies. For flow cells, the windows were used as received. For electrochemical flow cells, the windows were treated by HF, and then coated by electron-beam evaporated carbon (10 nm) and gold (15 nm). The gold-covered window was contacted by gold wires. Platinum wires were used as reference and counter electrodes. In the final step of assembly, the windows were glued to the cell body using Varian Torr seal epoxy, forming an electrolyte chamber of ~ 1 mm height. The contact between the gold film on the windows of the electrochemical cell and the gold wire was monitored during the curing process of the epoxy. Only cells with resistance between the two gold wires below 120 Ohm were used for electrochemical experiments. Using the Henke tables,[21] we calculated attenuation lengths ($I/I_0 = e^{-1}$) at 715 eV and 45° of 560, 40, 360 and 720 nm, for C,

Au, Si_3N_4 and water (i.e. ice), respectively. The resulting transmission through these components can be found in Figure S4A. About 82% of the intensity outside the sample cell was available at the window of the flow cell (schematic in Figure 1A) and 63% is available at the Au electrode surface of the electrochemical cell (schematic in Figure 1B). While incident X-rays penetrate deep into the bulk of the electrolyte, most of the detected fluorescence likely escaped from regions closer to the electrode due to reabsorption in the electrolyte and subsequent isotropic emission, of which a dwindeling fraction can be expected to arrive at the detector with increasing distance to the electrode.

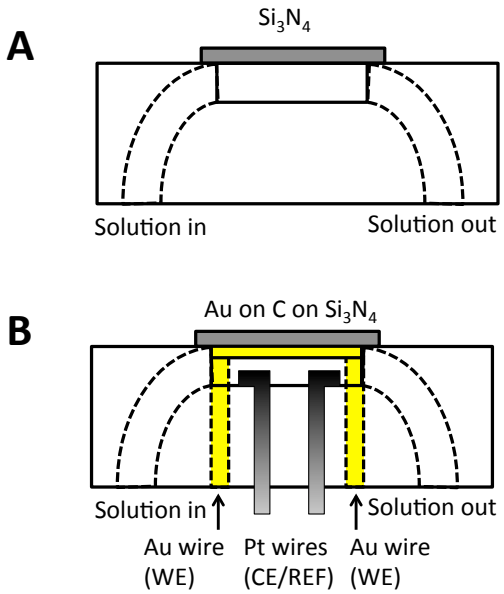

Figure 1. Schematics of the flow cells used in our experiments. (A) Flow cell and (B) electrochemical flow cell (WE = working electrode, CE = counter electrode, REF = reference electrode). X-rays enter and exit the cell through the Si_3N_4 window (grey) and are detected at an angle of 90° from the incident beam. We calculated an attenuation length ($I/I_0 = e^{-1}$) of 720 nm in ice as an approximation of the electrolyte (~ 1 mm deep), see text for further detail. However,

most of the detected fluorescence likely escaped from regions closer to the electrode due to reabsorption.

Electrolyte Preparation and Electrochemical Measurements

All solutions were prepared using deionized water (18.2 MΩ·cm) immediately before the XAS experiments. Ferrocyanide solution, $[Fe^{II}(CN)_6]^{4-}$, was prepared from $K_4Fe(CN)_6 \cdot 3H_2O$ (Sigma-Aldrich, 98.5 % purity) and ferricyanide solution, $[Fe^{III}(CN)_6]^{3-}$, was prepared from $K_3Fe(CN)_6$ (Sigma-Aldrich, 99 % purity) with concentrations of 0.1 M iron. The iron concentration was chosen high enough for good XAS signal and low enough to avoid precipitation of Prussian Blue or related coordination polymers. The kinetics of ferricyanide to ferrocyanide reduction and precipitation of iron-containing solids should depend on the iron concentration in ferri-ferrocyanide solutions. Therefore, the apparent onset of photo-damage would shift to a lower value for higher iron concentration. The pH of the solutions was adjusted from pH ~7 to pH 5 using sulfuric acid (Fisher Scientific, reagent grade), which impeded photo-damage (Figure S5A,B). We additionally added 0.1 M potassium sulfate (Fisher Scientific, reagent grade) as a supporting electrolyte to ferricyanide solutions to firstly provide excess potassium to bind free cyanide and secondly provide sulfate to coordinate with free iron, thus stabilizing it in solution (Figure S5C,D). Hydrochloric acid (1 M, Fisher Scientific, reagent grade) was used for cleaning the flow cells. All chemicals were used as received.

The potential in electrochemical experiments was controlled using a Voltalab PGZ-301 potentiostat and recorded simultaneously by the VoltaMaster4 software with high time resolution (< 0.1 s) compared to the XAS acquisition system (~ 1s), thereby avoiding synchronization issues. All potentials in this study are referenced to the thermodynamic potential of the ferri-

ferrocyanide redox couple (FCN) of 0.358 vs. SHE (standard hydrogen electrode) taken from the electrochemical series.[42] The electrolyte was drawn through the sample cell using a peristaltic pump (Cole Palmer Masterflex L/S Model 7528-10, speed setting 6 and 1.6 mm ID tubing) with a measured flow rate of 1.5 ml/min (25 μl/s). The volume below the window was about 10 mm^3, holding 10 μl solution, thus the solution maximally exposed to X-rays can be exchanged 2.5 times per second with this setting. The electrolyte reservoir was purged by argon gas during the measurements to minimize interference of oxygen reduction. The open-circuit voltage measured between the gold and platinum electrodes of the electrochemical cell was (0±25) mV vs. FCN in dark depending on the history of the electrode.

Results and Discussion

1. X-Ray Absorption of Ferri and Ferrocyanide Ions in the Flow Cell

Iron *L*-edge spectra of both ferricyanide and ferrocyanide solutions showed the spectral features expected for low-spin d^5 (i.e. $t_{2g}^5 e_g^0$) and low-spin d^6 (i.e. $t_{2g}^6 e_g^0$) iron[39] (Figure 2) using 0.1 M solutions adjusted to pH 5 (ferricyanide solution also contained potassium sulfate) in the flow cell (Figure 1A) with a flow rate of 1.5 ml/min and a photon flux density of 0.8×10^{11} $s^{-1}mm^{-2}$ in the cell. Under these conditions, our spectra compare well with those reported previously for powders of ferri- and ferrocyanide (Figure S6) in the absence of photo-damage,[22, 39, 43-46] as well as ferrocyanide solution.[19] We cannot confirm the discrepancies between powders and concentrated solution of an earlier report.[47] Minor differences between the powder and aqueous spectra in our measurements could be attributed to state-dependent decay effects, which cause fluorescence yield measurements to deviate from absorption cross sections.[48-50] The L_3 (704-718 eV, *a1-a3*) and L_2 (718-730 eV, *a4-a6*) edges of ferricyanide consisted of three main peaks each

while the L_3 and L_2 edges of ferrocyanide consisted of two peaks each (709-713 eV; *b1*, *b2* and 722-726 eV; *b3*, *b4*) due to π back-donation.[39] Fewer peaks of ferrocyanide (t_{2g}^6) as compared to ferricyanide (t_{2g}^5) can be attributed to filled t_{2g} orbitals, which reduces the number of multiplets. We assigned the observed peaks to electronic transitions (Table 1) based on the *L*-edge-like constant-incident-energy cuts though the RIXS plane with t_{2g} and e_g final states following Lundberg et al.[40] Specifically, peaks *a1*, *a4* correspond to 2*p* to t_{2g}^5 transitions in ferricyanide whereas peaks *a2*, *a3*/*a3'*, *a5*, *a6* correspond to 2*p* to e_g^0 transitions in ferricyanide and peaks *b1*, *b2*, *b3*, *a4* correspond to 2*p* to e_g^0 transitions in ferrocyanide.

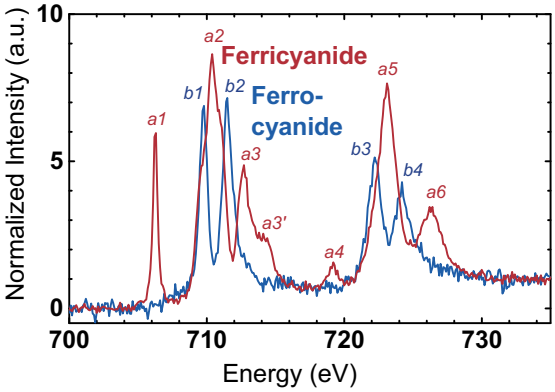

Figure 2. Iron *L*-edges of 0.1 M ferricyanide and 0.1 M ferrocyanide recorded in a flow cell (1.5 ml/min). All solutions were adjusted to pH 5 and ferricyanide solutions contained 0.1 M potassium sulfate. The assignment of peaks *a1*-*a6* and *b1*-*b4* can be found in Table 1. The photon flux density in the flow cell was 0.8×10^{11} $s^{-1}mm^{-2}$.

Table 1. Assignment of the peaks of ferricyanide, ferrocyanide and the ferric (hydr)oxide precipitate on the window.

Sample	Label	Energy (eV)	Character
Ferricyanide	*a1, a4*	706.2, 719.1	$2p \rightarrow t_{2g}^{5}$
	a2, a5	710.4, 723.2	$2p \rightarrow e_{g}^{0}$
	a3, a3', a6	712.7, 714.1, 726.2	$2p \rightarrow e_{g}^{0}$
Ferrocyanide	*b1, b3*	709.7, 722.2	$2p \rightarrow e_{g}^{0}$
	b2, b4	711.5, 724.2	$2p \rightarrow e_{g}^{0}$
Precipitate ferric (hydr)oxide	*c1, c4*	707.5, 720.7	d^5 high spin ($t_{2g}^{3} e_{g}^{2}$)
	c2, c5	709.1, 722.3	
	c3	711.6	

The character of transitions in ferri- and ferrocyanide was assigned based on ref. [40]. The character of the precipitate was assigned by comparison with a known d^5 high-spin (S=5/2) compound, α-FeOOH,[51] as shown in Figure S8.

At the L_3 edge of ferricyanide, *a3* has a shoulder *a3*' due to π and σ donation[39] at energies slightly higher than that of the main peak, while no shoulders were resolved for the corresponding peak at the L_2 edge. This difference can be attributed to the shorter core-hole life-time and resulting stronger intrinsic broadening of the L_2 edge as compared to the L_3 edge.[52] We focus on the discussion of L_3-edges herein due to their higher intrinsic resolution. Moreover, as the spectrum of ferrocyanide had no peaks below 710 eV, the peak intensity of *a1* (706.2 eV) of ferricyanide was used to follow the spectral changes due to photo-damage (section 2) and in time-resolved electrochemical experiments (section 3).

2. Study of Photo-Damage in the Flow Cell

Photo-damage (or radiation damage) is a known challenge during in-situ experiments with soft X-rays,[53] including work with liquids.[54] Unfortunately, photo-damage of the studied systems is mostly treated qualitatively and rarely quantified based on flux density or radiation dose. A notable exception is the recent work of Van Schooneveld and DeBeer,[22] which also includes quantification of radiation damage of ferricyanide powder. We decided against using the dose (energy deposited per mass of material) as recommended in ref. 22 for solids because the fluid dynamics of the electrolyte were unknown and instead used the experimentally accessible flux density. Common strategies to reduce photo-damage during in-situ experiments with liquids include increasing the size of the beam on the sample, e.g. by defocussing, and replacing the irradiated mass/volume continuously, e.g. flowing the liquid. Nagasaka et al.[33, 55] (schematic in Fig. S1) flowed at a rate of 5 ml/min, which replaced the liquid in the cell 3 times during the 3 s exposure at each energy step. Here, we determined the threshold flux density for photo-damage and state the flow rate of 1.5 ml/min, which was sufficient to replace the liquid 5 times during 2 s exposure at each energy step in our smaller cell.

Clear changes in the iron *L*-edge spectra of 0.1 M ferricyanide and 0.1 M ferrocyanide solutions were found relative to pristine solutions during a single XAS scan lasting 15 min at high flux (Figure 3). In addition, X-ray irradiation of ferricyanide and ferrocyanide produced solid precipitates on the window of the flow cell, which remained on the window after flushing the cell with copious amounts of DI water. Irradiated solutions of ferricyanide and ferrocyanide exhibited both their original features (*a1-a6* or *b1-b4*) and those of the precipitate (*c1-c5*), whose assignment can be found in Table 1. Subtracting appropriately scaled pristine spectra from the spectra of the respective irradiated solutions produces spectra identical to that of the precipitates

within noise (Figure S7), which indicates that the irradiated spectra can be described fully by the original solution and the precipitate. Furthermore, nearly identical precipitates formed when either ferricyanide or ferrocyanide solutions were irradiated (Figure S8), where minor differences might be caused by sample history and film thickness. The L_3-edge of the precipitate was characterized by two peaks, *c1* and *c2*, as well as a shoulder, *c3*, typical for high spin Fe^{III} ($t_{2g}^{3}e_{g}^{2}$) in ferric hydroxides[51, 56] and clearly distinct from the spectra of $Fe^{II}O$ and $Fe^{II,III}{}_3O_4$ (Figure S8). Please note that the L_3/L_2 ratio is different for the references spectra[56] as they were obtained using the inverse partial fluorescence yield (IPFY) rather than partial fluorescence yield (PFY) used herein. Among the iron oxides and hydroxides,[56] the separation between peaks *c1* and *c2* was closest to α-FeOOH, indicating comparable ligand field splitting (Figure S8). However, no conclusive assignment was achieved and we will refer to the precipitate as ferric (hydr)oxide, whose precipitation is in contrast to in-situ UV/vis experiments, where Prussian Blue is formed on the probed surface.[28-31] The X-ray absorption spectrum of Prussian Blue is a linear combination of ferri- and ferrocyanide.[57] Thus, we would expect to find peaks *a1-a6* in addition to *b1-b4* if appreciable amounts of Prussian Blue were formed. The absence of these peaks, particularly *a1*, in the precipitates supports that ferric (hydr)oxide rather than Prussian Blue was formed. This assignment is further supported by the fact that this hydroxide is thermodynamically stable in the Pourbaix diagram[58] under the electrochemical conditions (pH 5, cell potential ≥ 0.358 V vs. SHE) used in our experiments. It should be noted, however, that a blue deposit was visible on the periphery of the irradiated area (Figure S2), which might be Prussian Blue. In contrast, the color of the irradiated area is indistinguishable from ochrous α-FeOOH.[56] Thus, the spectral changes occurring during single XAS scans of ferri- and

ferrocyanide solutions illustrate that ferric (hydr)oxide precipitates from both solutions in the irradiated area.

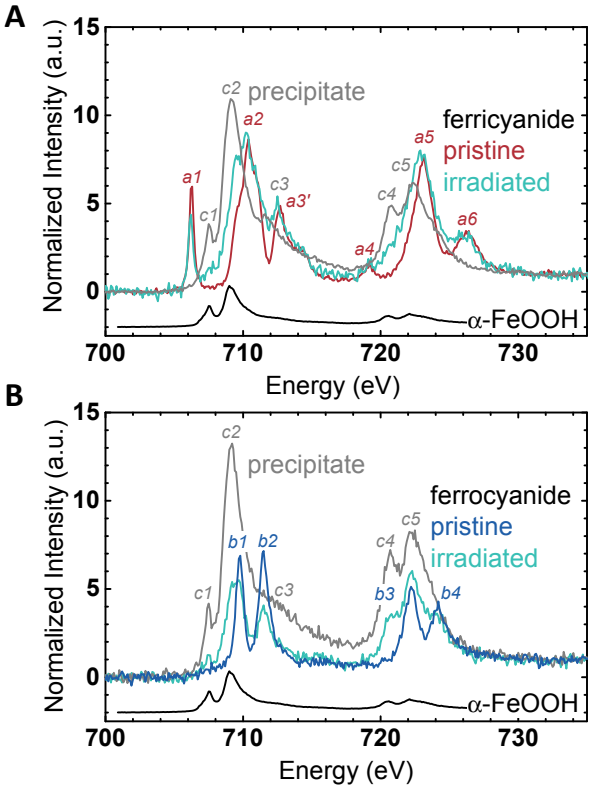

Figure 3. Iron *L*-edges of (A) 0.1 M pristine ferricyanide (red) and (B) 0.1 M pristine ferrocyanide (blue) compared to solutions of each species (teal) during a single scan (15 min) at high flux condition recorded in the flow cell (1.5 ml/min) and α-FeOOH (shifted and scaled for clarity).[56] All solutions were adjusted to pH 5 and ferricyanide solutions contained 0.1 M potassium sulfate. After irradiation at high flux in ferricyanide or ferrocyanide solutions, the cell was flushed with water and spectra of the precipitates (grey) were recorded using water-filled cells. The assignment of peaks *a1-a6*, *b1-b4* and *c1-c5* can be found in Table 1.

Precipitation of ferric (hydr)oxide has rarely been considered as a parasitic reaction during in-situ spectroscopy of ferri-ferrocyanide solutions. We hypothesize that ferric (hydr)oxide is formed due to cleavage of cyanide ligands and ionization of water by the intense ionizing X-ray radiation in the soft X-ray region, i.e. radiolysis. Water radicals (e.g. H*, OH*, H_2O_2) generated by ionizing radiation react with both ferri- and ferrocyanide and may replace the cyanide ligand (e.g. $Fe(CN)_6 \rightarrow Fe(CN)_5[OH_2]$).[24-25] The production of these radicals by soft X-rays (550 eV) in ice was previously reported[59] at flux densities comparable to those used in our experiments. A previous study based on FTIR spectroscopy suggests that more than one cyanide ligand could be lost and it was speculated that solute Fe^{3+} ions could be formed at neutral pH,[26] which can precipitate as iron hydroxide under these conditions.[58] In support of this, iron hydroxide was found previously after UV irradiation in basic solutions.[60] The Pourbaix diagram of the iron-water system[58] indicates that solid hydroxides are favored over aqueous Fe^{3+} and Fe^{2+} at pH 5, which is consistent with our XAS results for the precipitate on the window. Our soft XAS data provides direct evidence of iron hydroxide formation, presumably α-FeOOH, in mildly acidic ferri-ferrocyanide solutions after X-ray irradiation (Figure 3 and S8).

We further studied the onset of photo-damage at the iron L_3-edge by systematically increasing the photon flux on a solution of ferricyanide (Figure 4). The photon flux density was controlled between 0.8×10^{11} and 2.6×10^{11} $s^{-1}mm^{-2}$ by detuning the beamline undulator and adjusting the monochromator exit slit size between 10 and 15 μm, which had negligible effects on the energy resolution of the measurements and the spot size on the window. Using a flow rate of 1.5 ml/min, no time dependence was detected for subsequent scans at both the lowest and highest flux (Figure S10). Features of the precipitate, i.e. peaks, *c1, c2* and *c3* in the L_3-edge became clearly discernible within the estimated noise level at photon flux densities above 2.0×10^{11} $s^{-1}mm^{-2}$ and

increasingly visible during 30-min irradiation with each greater flux density, while the peak associated with ferricyanide (*a1*) decreased. The threshold identified here for a solution of ferricyanide is similar to the value reported for ice (2.5×10^{11} $s^{-1}mm^{-2}$)[59] and intermittent to the flux densities at which photo-reduction of organic Cu compounds was observed (10^{13} $s^{-1}mm^{-2}$) and prevented (10^{10} $s^{-1}mm^{-2}$) during 3.5 min irradiation.[61]

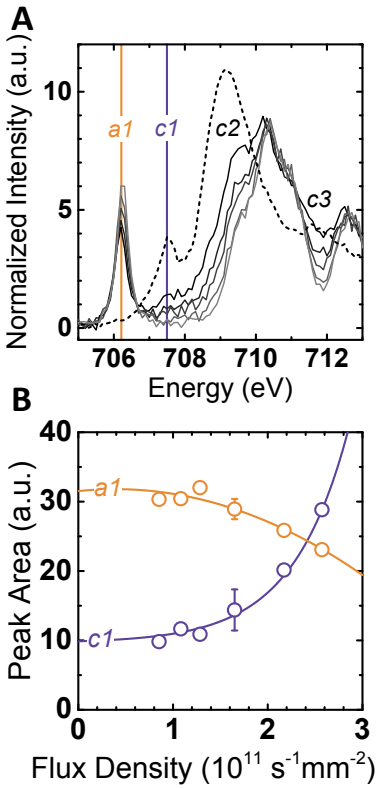

Figure 4. (A) Changes of the iron L_3-edge of ferricyanide with flux densities between 0.8×10^{11} and 2.6×10^{11} $s^{-1}mm^{-2}$ (light to dark; 5 scans $<10^{11}$ and 2 scans $>10^{11}$ $s^{-1}mm^{-2}$ of 15 min each) in the flow cell (1.5 ml/min) and the precipitate on the window (dashed line). The solution contained 0.1 M potassium sulfate and was adjusted to pH 5. (B) Dependence of the area under peaks *a1* and *c1* on the flux inside the cell. The assignment of these peaks can be found in Table 1 and the boundaries for integration in Figure S9. Error bars were only obtained for one

condition (1.6×10^{11} $s^{-1}mm^{-2}$) and show the standard deviation of 3 independent measurements (2 scans each). Lines were added to guide the eye.

The integrated intensities of *a1* and *c1* as a function of flux density are shown in Figure 4B. The observed non-linear trend with flux density can be attributed to the precipitation of iron hydroxide on the window, which increased the local density and thus reduced the penetration depth of incident X-rays. More significantly, a photon flux density of 0.2×10^{11} $s^{-1}mm^{-2}$ was sufficient to reduce the amplitude of peak *a1* over 5 subsequent scans (15 min each) when the flow was stopped (Figure S11). This observation suggests that it might be very challenging to minimize parasitic reactions of ferri-ferrocyanide redox during soft X-ray measurements as the onset flux density is exceptionally low and readily available at many soft X-ray beamlines (Table S1). In summary, we showed that the precipitation of ferric (hydr)oxide can occur at photon flux densities equal to or greater than 2.0×10^{11} $s^{-1}mm^{-2}$ at a flow rate of 1.5 ml/min with no time-dependent spectral changes between subsequent scans. In contrast, an order of magnitude lower flux density is sufficient for precipitation without flow and spectral changes depended on the duration of irradiation. Thus, the flow rate and flux density have to be balanced carefully to avoid photo-damage, while preserving useful XAS signal strengths, especially during time-dependent operando experiments.

3. Operando XAS of Electrochemical Ferricyanide Redox

Ferricyanide *L*-edges measured at open-circuit in the electrochemical flow cell were found comparable to those measured with the flow cell (Figure S12) for an identical flow rate of 1.5 ml/min. Photon flux densities lower than 0.8×10^{11} $s^{-1}mm^{-2}$ did not alter the open-circuit voltage

during the 15 min energy scan at 1.5 ml/min (Figure S13). Therefore, our electrochemical measurements were measured at this flux density and flow rate, which not only minimized the irradiation damage of the ferricyanide over time but also allowed sufficient XAS signal strength to capture dynamic changes in the L_3 edge associated with the redox between ferricyanide and ferrocyanide. With these parameters, we also did not observe abrupt changes in the iron fluorescence, which would be indicative of beam-induced bubble formation.

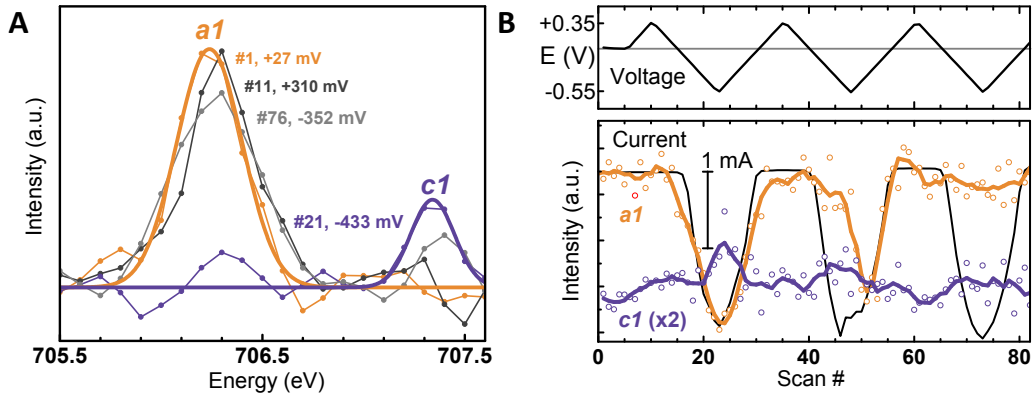

Figure 5. (A) Spectral changes of peaks *a1* and *c1* at the iron L_3-edge of ferricyanide during voltage sweeping between 0.35 and -0.55 V vs. FCN with 1 mV/s in the electrochemical flow cell (1.5 ml/min). The solution contained 0.1 M potassium sulfate and was adjusted to pH 5. The spectra were smoothed by a cubic spline algorithm covering 0.2 eV. Thick lines show Gaussian fits of peaks *a1* and *c1*. (B) Trends of the unsmoothed areas under peaks *a1* and *c1* (symbols) during 3 voltage cycles probed by 82 XAS scans and their smoothed trace (2^{nd} order polynomial smoothing, 8 point window). Black lines indicate current (bottom) and voltage (top), where the reversible potential of ferri-ferrocyanide (0 V vs. FCN) is indicated by a grey line. The duration of each scan was 72 ± 2 s. The photon flux density in the electrochemical flow cell was 0.8×10^{11} $s^{-1}mm^{-2}$.

The energy range containing peaks *a1* and *c1* in the L_3 edge of ferricyanide was scanned every 72 ± 2 s while the voltage was cycled from 0.35 to -0.55 V vs. FCN (Figure 5A). The measured reduction/oxidation currents (Figure 5B) below 0 V vs. FCN came from reduction of ferricyanide to ferrocyanide at the window electrode and vice-versa. As the initial solution only contained ferricyanide, there was no response in the electric current within the first 14 XAS scans (17 min). The area under peak *c1* was constant and increases slightly for positive voltages vs. FCN, while the area under peak *a1* appeared to be constant, likely due to the weaker dependence on ferric (hydr)oxide precipitation (Figure 4B). The constant *a1* and *c1* peak areas during the first 5 XAS scans (6 min) at open-circuit voltage suggested the absence of time-dependent spectral changes. Initial spectral changes during cyclic voltammetry would therefore be caused predominantly by polarization of the electrode. During the first cycle (scans 6 - 31), the area of peak *a1* followed the electric current very well (Figure 5B) and the minima coincided. The onset in the *a1* peak reduction for ferricyanide (scan 15) was found at negative voltages and prior to electrochemical reduction currents (Figure 5B). The latter observation suggested photo-damage of ferricyanide, which is supported by the increased area of peak *c1*, indicating the formation of the ferric (hydr)oxide precipitate on the window as discussed previously. Indeed, a spectrum with the characteristic features of the ferric (hydr)oxide precipitate was found after the CV experiment in a cell flushed and filled with water (Figure S14). During the second cycle (scans 32 - 57), the peak area reduction of *a1* for ferricyanide was much delayed relative to the reduction current, and no change was found for peak *a1* in the third cycle (scans 58 - 83), which can be attributed to the passivation of the X-ray-probed electrode area by iron (hydr)oxide precipitation. The electrochemical current was not affected by the passivation because the area probed by XAS is ~0.5 % of the total electrochemically active surface (Figure S2), which is common for operando

(photo)electrochemical measurements where the electrode is on the window.[62-65] Interestingly, peak *c1* was maximal when peak *a1* vanished, i.e. when ferricyanide was fully reduced to ferrocyanide near the electrode during the first cycle (scans 6 - 31; Figure 5), indicating that the ferri-ferrocyanide redox might correlate with the formation of ferric (hydr)oxide, such that negative (reducing) voltages promoted its precipitation.

In summary, in-situ measurements with the flow cell were comparable to operando measurements with the electrochemical flow cell at open-circuit for photon flux densities below 10^{11} $s^{-1}mm^{-2}$. At an identical flow rate of 1.5 ml/min, spectral changes were not time-dependent under these conditions and the formation of iron (hydr)oxide was not observed on the window electrode of both cells. However, increasing coverage by the precipitate was witnessed after voltage cycling between 0.35 V and -0.55 V vs. FCN, which impeded the electrochemical ferri-ferrocyanide redox observed by XAS. The coincidence between ferri-ferrocyanide redox and the parasitic reaction showed that photochemical and electrochemical reactions need to be considered for damage-free during operando measurements. We argued that the precipitation of iron (hydr)oxide at open-circuit may relate to the formation of radicals by soft X-rays and that reducing voltages may additionally promote precipitation during cyclic voltammetry. It is conceivable that aqueous Fe^{II} preferentially reacts with the generated radicals to produce the observed $Fe^{III}OOH$. The flux density of 2.5×10^{11} $s^{-1}mm^{-2}$ (ref. 59) to generate radicals in aqueous electrolytes is readily obtainable at soft X-ray beamlines around the world (Table S1). Unfortunately, flux densities or radiation doses are rarely reported, even when operating conditions were optimized. In the absence of explicit testing for photo-damage at open-circuit, it is likely that these radicals are produced in aqueous electrolytes by ionizing soft X-ray radiation,

which raises the important question of how they interact with soluble species or electrode surfaces in electrochemical operando measurements.

Conclusions

We studied the ferri-ferrocyanide redox by in-situ XAS both in an electrode-free flow cell and an electrochemical flow cell. The spectra of ferricyanide and ferrocyanide solutions in the flow cell agreed with those of corresponding powders under photon fluxes below the threshold of radiolysis. At photon flux densities equal to and exceeding 2×10^{11} $s^{-1}mm^{-2}$ at a flow rate of 1.5 ml/min, the precipitation of passivating ferric (hydr)oxide on the Au/Si_3N_4 window occurred as a side reaction at open-circuit. However, the electrochemical ferri-ferrocyanide redox by voltage cycling coincided with (hydr)oxide precipitation below a flux density of 10^{11} $s^{-1}mm^{-2}$ at identical flow rate. The precipitate passivated the electrode in the irradiated area so that ferri-ferrocyanide redox could not be detected by XAS. In contrast, the effect on the electrochemical current was negligible because less than 0.5 % of the window area was irradiated. Our work highlighted the importance of considering both electrochemical and photochemical effects when designing soft X-ray operando experiments to gain insight into electrochemical systems free of beam-induced damage. Technical improvements such as continuous scanning of beamline energy and fast readout of detector electronics are important for optimization of the experiment, reducing the radiation dose absorbed by the sample. Probing electrochemical reactions with ionizing radiation thus was accompanied by additional challenges but the extra effort could be justified as such experiments may shed light on charge transfer and chemistry of active sites in energy and health research.

AUTHOR INFORMATION

Corresponding Authors

*Marcel Risch, Massachusetts Institute of Technology, 77 Massachusetts Ave, Cambridge, MA 02139, +1-617-253-0536, email: mrisch@mit.edu

*Yang Shao-Horn, Massachusetts Institute of Technology, 77 Massachusetts Ave, Cambridge, MA 02139, +1-617-253-2259, email: shaohorn@mit.edu

⊥Permanent Address for Sayed Youssef Sayed:
Department of Chemistry, Faculty of Science, Cairo University, Giza 12613, Egypt.

Author Contributions

The manuscript was written through contributions of all authors. All authors have given approval to the final version of the manuscript.

ACKNOWLEDGMENT

This work was supported in part by the MRSEC Program of the National Science Foundation under award number DMR-0819762, the DOE Hydrogen Initiative Program under Award DE-FG02-05ER15728, the Skoltech-MIT Center for Electrochemical Energy Storage. This work made use of the MIT MRSEC Shared Experimental Facilities supported by the National Science Foundation under award number DMR-0819762. Research described in this paper was performed at the Canadian Light Source, which is supported by the Canadian Foundation for Innovation, Natural Sciences and Engineering Research Council of Canada, the University of Saskatchewan, the Government of Saskatchewan, Western Economic Diversification Canada, the National Research Council Canada, and the Canadian Institutes of Health Research. K.A.S. was

supported in part by the National Science Foundation Graduate Research Fellowship under Grant no. DGE-1122374. S.Y.S. is thankful for the support of a postdoctoral fellowship from the Natural Sciences and Engineering Research Council (NSERC) of Canada. We thank Dr. Xiao (Renshaw) Wang for help with the design of the TOC graphic and Figure S1A.

Supporting Information. Postmortem picture of the cell window, additional X-ray absorption spectra and electrochemical data. This information is available free of charge via the Internet at http://pubs.acs.org.

REFERENCES

1. DeAngelis, T. P.; Heineman, W. R. An Electrochemical Experiment Using an Optically Transparent Thin Layer Electrode. *J. Chem. Educ.* **1976,** *53* (9), 594.
2. Huang, T. H.; Salter, G.; Kahn, S. L.; Gindt, Y. M. Redox Titration of Ferricyanide to Ferrocyanide with Ascorbic Acid: Illustrating the Nernst Equation and Beer–Lambert Law. *J. Chem. Educ.* **2007,** *84* (9), 1461.
3. Van Benschoten, J. J.; Lewis, J. Y.; Heineman, W. R.; Roston, D. A.; Kissinger, P. T. Cyclic Voltammetry Experiment. *J. Chem. Educ.* **1983,** *60* (9), 772.
4. Galizzioli, D.; Trasatti, S. Work Function, Electronegativity, and Electrochemical Behaviour of Metals: IV. Simple Electron Exchange Reactions. Fe^{2+}/F^{e3+} Redox Couple. *J. Electroanal. Chem.* **1973,** *44* (3), 367-388.
5. Stoerzinger, K. A.; Risch, M.; Suntivich, J.; Lu, W. M.; Zhou, J.; Biegalski, M. D.; Christen, H. M.; Ariando; Venkatesan, T.; Shao-Horn, Y. Oxygen Electrocatalysis on (001)-Oriented Manganese Perovskite Films: Mn Valency and Charge Transfer at the Nanoscale. *Energy Environ. Sci.* **2013,** *6* (5), 1582-1588.
6. Miyahara, Y.; Miyazaki, K.; Fukutsuka, T.; Abe, T. Catalytic Roles of Perovskite Oxides in Electrochemical Oxygen Reactions in Alkaline Media. *J. Electrochem. Soc.* **2014,** *161* (6), F694-F697.
7. Seger, B.; Pedersen, T.; Laursen, A. B.; Vesborg, P. C. K.; Hansen, O.; Chorkendorff, I. Using TiO_2 as a Conductive Protective Layer for Photocathodic H_2 Evolution. *J. Am. Chem. Soc.* **2013,** *135* (3), 1057-1064.
8. Lu, Y.; Goodenough, J. B. Rechargeable Alkali-Ion Cathode-Flow Battery. *J. Mater. Chem.* **2011,** *21* (27), 10113-10117.
9. Mua, Y.; Quickenden, T. I. Power Conversion Efficiency, Electrode Separation, and Overpotential in the Ferricyanide/Ferrocyanide Thermogalvanic Cell. *J. Electrochem. Soc.* **1996,** *143* (8), 2558-2564.
10. Burrows, B. Discharge Behavior of Redox Thermogalvanic Cells. *J. Electrochem. Soc.* **1976,** *123* (2), 154-159.

11. Romano, M. S.; Li, N.; Antiohos, D.; Razal, J. M.; Nattestad, A.; Beirne, S.; Fang, S.; Chen, Y.; Jalili, R.; Wallace, G. G., et al. Carbon Nanotube – Reduced Graphene Oxide Composites for Thermal Energy Harvesting Applications. *Adv. Mater.* **2013,** *25* (45), 6602-6606.
12. Zhu, X.; Yang, H.; Ai, X. Possible Use of Ferrocyanide as a Redox Additive for Prevention of Electrolyte Decomposition in Overcharged Nickel Batteries. *Electrochim. Acta* **2003,** *48* (27), 4033-4037.
13. Daeneke, T.; Uemura, Y.; Duffy, N. W.; Mozer, A. J.; Koumura, N.; Bach, U.; Spiccia, L. Aqueous Dye-Sensitized Solar Cell Electrolytes Based on the Ferricyanide–Ferrocyanide Redox Couple. *Adv. Mater.* **2012,** *24* (9), 1222-1225.
14. Ming, T.; Suntivich, J.; May, K. J.; Stoerzinger, K. A.; Kim, D. H.; Shao-Horn, Y. Visible Light Photo-Oxidation in Au Nanoparticle Sensitized $SrTiO_3$:Nb Photoanode. *J. Phys. Chem. C* **2013,** *117* (30), 15532-15539.
15. Lee, T.; Jiang, Y.; Rose-Petruck, C. G.; Benesch, F. Ultrafast Tabletop Laser-Pump–X-Ray Probe Measurement of Solvated $Fe(CN)_6^{4-}$. *J. Chem. Phys.* **2005,** *122* (8), 084506.
16. Reinhard, M.; Penfold, T. J.; Lima, F. A.; Rittmann, J.; Rittmann-Frank, M. H.; Abela, R.; Tavernelli, I.; Rothlisberger, U.; Milne, C. J.; Chergui, M. Photooxidation and Photoaquation of Iron Hexacyanide in Aqueous Solution: A Picosecond X-Ray Absorption Study. *Structural Dynamics* **2014,** *1* (2), 024901.
17. Inada, Y.; Hayashi, H.; Funahashi, S.; Nomura, M. Time-Resolved Stopped-Flow X-Ray Absorption Fine Structure System Using Synchrotron Radiation for Fast Reactions in Solution. *Rev. Sci. Instrum.* **1997,** *68* (8), 2973-2977.
18. Penfold, T. J.; Reinhard, M.; Rittmann-Frank, M. H.; Tavernelli, I.; Rothlisberger, U.; Milne, C. J.; Glatzel, P.; Chergui, M. X-Ray Spectroscopic Study of Solvent Effects on the Ferrous and Ferric Hexacyanide Anions. *J. Phys. Chem. A* **2014,** *118* (40), 9411-9418.
19. Engel, N.; Bokarev, S. I.; Suljoti, E.; Garcia-Diez, R.; Lange, K. M.; Atak, K.; Golnak, R.; Kothe, A.; Dantz, M.; Kühn, O., et al. Chemical Bonding in Aqueous Ferrocyanide: Experimental and Theoretical X-Ray Spectroscopic Study. *J. Phys. Chem. B* **2014,** *118* (6), 1555-1563.
20. Aziz, E. F.; Rittmann-Frank, M. H.; Lange, K. M.; Bonhommeau, S.; Chergui, M. Charge Transfer to Solvent Identified Using Dark Channel Fluorescence-Yield L-Edge Spectroscopy. *Nat Chem* **2010,** *2* (10), 853-857.
21. Henke, B. L.; Gullikson, E. M.; Davis, J. C. X-Ray Interactions: Photoabsorption, Scattering, Transmission, and Reflection at E = 50-30,000 eV, Z = 1-92. *At. Data Nucl. Data Tables* **1993,** *54* (2), 181-342.
22. van Schooneveld, M. M.; DeBeer, S. A Close Look at Dose: Toward L-Edge XAS Spectral Uniformity, Dose Quantification and Prediction of Metal Ion Photoreduction. *J. Electron. Spectrosc. Relat. Phenom.* **2015,** *198*, 31-56.
23. Asperger, S. Kinetics of the Decomposition of Potassium Ferrocyanide in Ultra-Violet Light. *T. Faraday Soc.* **1952,** *48*, 617-624.
24. Zehavi, D.; Rabani, J. Pulse Radiolysis of the Aqueous Ferro-Ferricyanide System. I. Reactions of OH, HO_2, and O^{2-} Radicals. *J. Phys. Chem.* **1972,** *76* (25), 3703-3709.
25. Zehavi, D.; Rabani, J. Pulse Radiolysis of the Aqueous Ferro-Ferricyanide System. II. Reactions of Hydrogen Atoms and Hydrated Electrons with Ferrocyanide and Ferricyanide Ions. *J. Phys. Chem.* **1974,** *78* (14), 1368-1373.

26. Le Caër, S.; Vigneron, G.; Renault, J. P.; Pommeret, S. First Coupling between a LINAC and FT-IR Spectroscopy: The Aqueous Ferrocyanide System. *Chem. Phys. Lett.* **2006,** *426* (1–3), 71-76.
27. Arellano, C. A. P.; Martínez, S. S. Effects of pH on the Degradation of Aqueous Ferricyanide by Photolysis and Photocatalysis under Solar Radiation. *Sol. Energy Mater. Sol. Cells* **2010,** *94* (2), 327-332.
28. Pharr, C. M.; Griffiths, P. R. Infrared Spectroelectrochemical Analysis of Adsorbed Hexacyanoferrate Species Formed During Potential Cycling in the Ferrocyanide/Ferricyanide Redox Couple. *Anal. Chem.* **1997,** *69* (22), 4673-4679.
29. Pharr, C. M.; Griffiths, P. R. Step-Scan FT-IR Spectroelectrochemical Analysis of Surface and Solution Species in the Ferricyanide/Ferrocyanide Redox Couple. *Anal. Chem.* **1997,** *69* (22), 4665-4672.
30. Kunimatsu, K.; Shigematsu, Y.; Uosaki, K.; Kita, H. Study of the $Fe(CN)^{3-}_6/Fe(CN)^{4-}_6$ Redox System on Pt by EMIRS: Part I. Infrared Spectra of the Intermediates in the Charge Transfer. *J. Electroanal. Chem.* **1989,** *262* (1–2), 195-209.
31. Huang, W.; McCreery, R. Electron Transfer Kinetics of $Fe(CN)_6^{3-4-}$ on Laser-Activated and CN^--Modified Pt Electrodes. *J. Electroanal. Chem.* **1992,** *326* (1–2), 1-12.
32. de Tacconi, N. R.; Rajeshwar, K.; Lezna, R. O. Metal Hexacyanoferrates: Electrosynthesis, in Situ Characterization, and Applications. *Chem. Mater.* **2003,** *15* (16), 3046-3062.
33. Nagasaka, M.; Yuzawa, H.; Horigome, T.; Hitchcock, A. P.; Kosugi, N. Electrochemical Reaction of Aqueous Iron Sulfate Solutions Studied by Fe L-Edge Soft X-Ray Absorption Spectroscopy. *J. Phys. Chem. C* **2013,** *117* (32), 16343-16348.
34. Regier, T.; Krochak, J.; Sham, T. K.; Hu, Y. F.; Thompson, J.; Blyth, R. I. R. Performance and Capabilities of the Canadian Dragon: The SGM Beamline at the Canadian Light Source. *Nucl. Instrum. Meth. A* **2007,** *582* (1), 93-95.
35. We note that an angle of exactly 45º would have resulted in unwanted detection of the reflected beam, which was not observed. .
36. Hitchcock, A. P.; Brion, C. E. K-Shell Excitation Spectra of CO, N_2 and O_2. *J. Electron. Spectrosc. Relat. Phenom.* **1980,** *18* (1), 1-21.
37. Gullikson, E. M.; Korde, R.; Canfield, L. R.; Vest, R. E. Stable Silicon Photodiodes for Absolute Intensity Measurements in the VUV and Soft X-Ray Regions. *J. Electron. Spectrosc. Relat. Phenom.* **1996,** *80*, 313-316.
38. de Groot, F. High-Resolution X-Ray Emission and X-Ray Absorption Spectroscopy. *Chem. Rev.* **2001,** *101* (6), 1779-1808.
39. Hocking, R. K.; Wasinger, E. C.; de Groot, F. M. F.; Hodgson, K. O.; Hedman, B.; Solomon, E. I. Fe L-Edge XAS Studies of $K_4[Fe(CN)_6]$ and $K_3[Fe(CN)_6]$: A Direct Probe of Back-Bonding. *J. Am. Chem. Soc.* **2006,** *128* (32), 10442-10451.
40. Lundberg, M.; Kroll, T.; DeBeer, S.; Bergmann, U.; Wilson, S. A.; Glatzel, P.; Nordlund, D.; Hedman, B.; Hodgson, K. O.; Solomon, E. I. Metal–Ligand Covalency of Iron Complexes from High-Resolution Resonant Inelastic X-Ray Scattering. *J. Am. Chem. Soc.* **2013,** *135* (45), 17121-17134.
41. Phillips, C. L.; Regier, T. Z.; Peak, D. Aqueous Cu(II)–Organic Complexation Studied in Situ Using Soft X-Ray and Vibrational Spectroscopies. *Environ. Sci. Technol.* **2013,** *47* (24), 14290-14297.

42. Vanysek, P., Electrochemical Series. In *CRC Handbook of Chemsitry and Physics*, 95th ed.; Taylor and Francis: 2014; Vol. 5, pp 80-89.
43. Cartier dit Moulin, C.; Villain, F.; Bleuzen, A.; Arrio, M.-A.; Sainctavit, P.; Lomenech, C.; Escax, V.; Baudelet, F.; Dartyge, E.; Gallet, J.-J., et al. Photoinduced Ferrimagnetic Systems in Prussian Blue Analogues $CI_xCo_4[Fe(CN)_6]Y$ (CI = Alkali Cation). 2. X-Ray Absorption Spectroscopy of the Metastable State. *J. Am. Chem. Soc.* **2000,** *122* (28), 6653-6658.
44. Collison, D.; Garner, C. D.; McGrath, C. M.; Mosselmans, J. F. W.; Roper, M. D.; Seddon, J. M. W.; Sinn, E.; Young, N. A. Soft X-Ray Photochemistry at the $L_{2,3}$-Edges in $K_3[Fe(CN)_6]$, $[Co(acac)_3]$ and $[Cp_2Fe][BF_4]$. *Journal of Synchrotron Radiation* **1999,** *6* (3), 585-587.
45. George, S. J.; Fu, J.; Guo, Y.; Drury, O. B.; Friedrich, S.; Rauchfuss, T.; Volkers, P. I.; Peters, J. C.; Scott, V.; Brown, S. D., et al. X-Ray Photochemistry in Iron Complexes from Fe(0) to Fe(IV) – Can a Bug Become a Feature? *Inorg. Chim. Acta* **2008,** *361* (4), 1157-1165.
46. Yoshinori, K.; Kotaro, I.; Tomoyuki, M.; Hiroko, T.; Shin-ichi, O.; Toshiaki, I. First Observation of Soft X-Ray Induced Phase Transition of $Rbmn[Fe(CN)_6]$ Studied by Fe L-Edge X-Ray Absorption Spectroscopy. *Journal of Physics: Conference Series* **2009,** *148* (1), 012032.
47. Freiwald, M.; Cramm, S.; Eberhardt, W.; Eisebitt, S. Soft X-Ray Absorption Spectroscopy in Liquid Environments. *J. Electron. Spectrosc. Relat. Phenom.* **2004,** *137–140*, 413-416.
48. Green, R. J.; Peak, D.; Achkar, A. J.; Tse, J. S.; Moewes, A.; Hawthorn, D. G.; Regier, T. Z. Comment on "State-Dependent Electron Delocalization Dynamics at the Solute-Solvent Interface: Soft-X-Ray Absorption Spectroscopy and Ab initio Calculations". *Phys. Rev. Lett.* **2014,** *112* (12), 129301.
49. Miedema, P. S.; Wernet, P.; Föhlisch, A. State-Dependent Fluorescence Yields through the Core-Valence Coulomb Exchange Parameter. *Phys. Rev. A* **2014,** *89* (5), 052507.
50. de Groot, F. M. F. Dips and Peaks in Fluorescence Yield X-Ray Absorption Are Due to State-Dependent Decay. *Nat Chem* **2012,** *4* (10), 766-767.
51. Forsyth, J. B.; Hedley, I. G.; Johnson, C. E. The Magnetic Structure and Hyperfine Field of Goethite (α-FeOOH). *J. Phys. C Solid State* **1968,** *1* (1), 179.
52. Fuggle, J. C.; Inglesfield, J. E., Introduction. In *Unoccupied Electronic States*, Fuggle, J. C.; Inglesfield, J. E., Eds. Springer: 1992; Vol. 69.
53. Wang, J.; Morin, C.; Li, L.; Hitchcock, A. P.; Scholl, A.; Doran, A. Radiation Damage in Soft X-Ray Microscopy. *J. Electron. Spectrosc. Relat. Phenom.* **2009,** *170* (1–3), 25-36.
54. Lange, K. M.; Aziz, E. F. Electronic Structure of Ions and Molecules in Solution: A View from Modern Soft X-Ray Spectroscopies. *Chem. Soc. Rev.* **2013,** *42* (16), 6840-6859.
55. Nagasaka, M.; Hatsui, T.; Horigome, T.; Hamamura, Y.; Kosugi, N. Development of a Liquid Flow Cell to Measure Soft X-Ray Absorption in Transmission Mode: A Test for Liquid Water. *J. Electron. Spectrosc. Relat. Phenom.* **2010,** *177* (2–3), 130-134.
56. Peak, D.; Regier, T. Direct Observation of Tetrahedrally Coordinated Fe(III) in Ferrihydrite. *Environ. Sci. Technol.* **2012,** *46* (6), 3163-3168.
57. Glatzel, P.; Jacquamet, L.; Bergmann, U.; de Groot, F. M. F.; Cramer, S. P. Site-Selective EXAFS in Mixed-Valence Compounds Using High-Resolution Fluorescence Detection: A Study of Iron in Prussian Blue. *Inorg. Chem.* **2002,** *41* (12), 3121-3127.

58. Pourbaix, M., *Atlas of Electrochemical Equilibria in Aqueous Solutions*. 2nd ed.; National Association of Corrosion: 1974.
59. Laffon, C.; Lacombe, S.; Bournel, F.; Parent, P. Radiation Effects in Water Ice: A Near-Edge X-Ray Absorption Fine Structure Study. *J. Chem. Phys.* **2006,** *125* (20), 204714.
60. Fuller, M.; Lebrocq, K.; Leslie, E.; Wilson, I. The Photolysis of Aqueous-Solutions of Potassium Hexacyanoferrate(III). *Aust. J. Chem.* **1986,** *39* (9), 1411-1419.
61. Yang, J.; Regier, T.; Dynes, J. J.; Wang, J.; Shi, J.; Peak, D.; Zhao, Y.; Hu, T.; Chen, Y.; Tse, J. S. Soft X-Ray Induced Photoreduction of Organic Cu(II) Compounds Probed by X-Ray Absorption Near-Edge (XANES) Spectroscopy. *Anal. Chem.* **2011,** *83* (20), 7856-7862.
62. Schwanke, C.; Golnak, R.; Xiao, J.; Lange, K. M. Electrochemical Flowcell for in-Situ Investigations by Soft X-Ray Absorption and Emission Spectroscopy. *Rev. Sci. Instrum.* **2014,** *85* (10), 103120.
63. Arthur, T. S.; Glans, P.-A.; Matsui, M.; Zhang, R.; Ma, B.; Guo, J. Mg Deposition Observed by in Situ Electrochemical Mg K-Edge X-Ray Absorption Spectroscopy. *Electrochem. Commun.* **2012,** *24*, 43-46.
64. Velasco-Velez, J.-J.; Wu, C. H.; Pascal, T. A.; Wan, L. F.; Guo, J.; Prendergast, D.; Salmeron, M. The Structure of Interfacial Water on Gold Electrodes Studied by X-Ray Absorption Spectroscopy. *Science* **2014,** *346* (6211), 831-834.
65. Braun, A.; Sivula, K.; Bora, D. K.; Zhu, J.; Zhang, L.; Grätzel, M.; Guo, J.; Constable, E. C. Direct Observation of Two Electron Holes in a Hematite Photoanode During Photoelectrochemical Water Splitting. *J. Phys. Chem. C* **2012,** *116* (32), 16870-16875.

Table of Contents (TOC) Image